PCCP

Accepted Manuscript

ROYAL SOCIETY OF CHEMISTRY

www.rsc.org/pccp

Dynamic propensity as an indicator of heterogeneity in room-temperature ionic liquids

Daekeon Kim, Daun Jeong,† and YounJoon Jung*

Department of Chemistry, Seoul National University, 151-747, Seoul, Korea

(Dated: July 31, 2014)

Abstract

We investigate the dynamic propensity in a coarse-grained model of a room-temperature ionic liquid via molecular dynamics simulations. Dynamic propensity is defined as the average of squared displacements for each ion during a given time interval over the isoconfigurational ensemble. As the temperature is lowered, distributions of the dynamic propensity develop fat tails at high values, indicating the presence of dynamic heterogeneity in the system. The increase in the heterogeneity for the cation is more evident than that for the anion, and a high propensity exhibits a large variance in the isoconfigurational ensemble, implying that dynamic propensity is related to ions' motions at a large length scale, rather than a direct measure of the individual ion dynamics. In addition, large non-Gaussian parameters observed for small dynamic propensities reveal intermittent dynamical behaviors of ions. In order to reveal the origin of the dynamic heterogeneity in a room-temperature ionic liquid, a possible correlation between the mobility and dynamic propensity is further probed. It is observed that spatial distributions of the dynamic propensity coincide with those of the mobility. The results suggest a possible connection between the structure and heterogeneous dynamics on large length scales.

† Present adress: Samsung Advanced Institute of Technology, 446-712, Yongin-si, Gyeonggi-do, Korea

* Corresponding author. E-mail: yjjung@snu.ac.kr

I. INTRODUCTION

Room-temperature ionic liquids (RTILs) are molten organic salts made of bulky cations and non-coordinating anions [1–3]. Numerous combinations of cations and anions can be designed to have superior physicochemical properties necessary in various applications. For example, nonvolatility and high thermal stability make RTILs a promising alternative to volatile organic solvents or electrolytes in applications for fuel cells [4], solar cells [5], and supercapacitor devices [6]. However, higher viscosity of RTILs compared with conventional volatile solvents may deteriorate the performance of ionic liquid-based electrolytes. Viscosity of RTILs varies in a wide range, as we choose different ionic species or add other solvent molecules [7]. It also increases abruptly as the temperature is lowered, signaling the presence of a glass transition [8]. Due to strong interactions between ions, RTILs exhibit viscous dynamics even at room temperatures, which is strikingly different from normal liquids. This aspect has provoked intense theoretical interest as well as practical issues.

Viscous dynamics in RTILs have been studied theoretically through molecular dynamics simulations by many researchers [9–18]. Solvation and rotational dynamics of the solute are found to be described by the nonexponential relaxation in accordance with the experimental results [19–23]. Translational dynamics of the ions are characterized with the nonexponential structural relaxation, subdiffusive behavior, violation of the Stokes-Einstein relation, and the decoupling phenomena. These phenomena appear clearly as the temperature is lowered [15].

As a matter of fact, the aforementioned phenomena in the translational dynamics have been observed previously in various models of supercooled liquids [24–30], where the Coulomb interactions are absent. It is quite interesting that such dynamic features seem to be universal and independent of the types of molecular interactions present in viscous liquids when approaching the glass transition.

These phenomena can be understood as arising from the dynamic correlation in the spatio-temporal trajectories of supercooled liquids [31, 32], dubbed dynamic heterogeneity, and it manifests itself as the coexistence of mobile and immobile regions in supercooled liquids. The dynamic heterogeneity also yields the coupling behavior of exchange and persistence times as verified earlier [15, 25].

Although understanding the link between structure and dynamics has been a central question in supercooled liquids and been investigated by many different researchers using various tools [33], it still remains an open question to identify the exact mechanism of the development of the dynamic correlation. For example, mechanisms based on purely fluctuation-dominated dynamics as well as those emphasizing dominant influence of the structure have been proposed. To elucidate a possible structural origin of the resulting dynamics, a concept of dynamic propensity has been proposed recently as a measure of an individual particle's movement in a two-dimensional model of supercooled liquids [34–36]. Statistical distributions and spatial patterns of the dynamic propensity have been investigated previously [37–39]. It is observed that the distribution of the dynamic propensity markedly deviates from a Gaussian behavior, displaying a fat tail at high propensities in a supercooled regime. Since the dynamic propensity may encode structural information related to dynamic heterogeneity, it has attracted much attention recently, in particular, regarding to its predictability of the long time dynamics [37–39].

As mentioned above, dynamics of RTILs at low temperatures are phenomenologically similar to those of supercooled liquids, reflecting the presence of the dynamic heterogeneity. In order to further investigate the dynamical nature of RTILs, we examine statistical properties of the dynamic propensity and discuss nature of the intermittent motions of ions at low temperatures by monitoring how the dynamic propensity reflects heterogeneous dynamics in RTILs. We believe

this work is the first application of the concept of dynamic propensity to complex molecular liquids such as RTILs. To connect the dynamic propensity and actual dynamics, we define mobility for each ion, describing dynamic heterogeneity in a single run starting from the same initial positions. We find that the dynamic propensity has weak correlation with individual particle's movement. Instead, spatial patterns of mobile and immobile regions have correlations with the dynamic propensity patterns, and these collective dynamical fluctuations have a non-local structural origin.

This paper is organized as follows: In Sec. II, we briefly introduce the dynamic propensity in the isoconfigurational ensemble. A coarse-grained model of an RTIL and simulation methods are summarized in Sec. III. In Sec. IV, we analyze of the dynamic propensity and investigate its correlation with the mobility. Finally, we conclude in Sec. V.

II. ISOCONFIGURATIONAL ENSEMBLE AND DYNAMIC PROPENSITY

In this section, we briefly introduce isoconfigurational (IC) ensemble and dynamic propensity, which have been employed to examine the heterogeneity of various supercooled liquid systems [34–42]. An equilibrium configuration of molecules in a liquid can be achieved with numerous different sets of momenta following the Maxwell-Boltzmann (MB) distribution in phase space. Such a subset of the equilibrium ensemble defines the IC ensemble, whose the members have the same configuration but different momenta. When we employ the IC ensemble for calculating physical properties by using the ensemble average, variations in the initial momenta are averaged out. Thus, dynamical quantities for each constituent particle in the IC ensemble would provide a clue to structural influence on the resultant dynamics, especially in glass forming liquids where significant movements occur

sporadically. With this respect, the dynamic propensity p_i of the i-th particle is introduced to investigate dynamic heterogeneity, and it represents individual particle's tendency to move for a given configuration [34–36], defined as

$$p_i \equiv \langle |\mathbf{r}_i(t^*) - \mathbf{r}_i(0)|^2 \rangle_{\mathrm{IC}}, \tag{1}$$

where $\langle \cdots \rangle_{\mathrm{IC}}$ denotes the average over the IC ensemble for a given initial configuration. The time interval t^* has been usually chosen on the order of τ_α, which is the structural relaxation time determined from the characteristic time scale of the self-intermediate scattering function $F_s(q_0, t) \equiv \langle \exp[i\mathbf{q_0} \cdot \{\mathbf{r}(t) - \mathbf{r}(0)\}] \rangle$, such that $F_s(q_0, \tau_\alpha) = 1/e$. Here, $\langle \cdots \rangle$ denotes the average over particles and equilibrium ensembles and q_0 represents the wavevector corresponding to the first peak position of the static structure factor for all molecular species.

Previously, Harrowell and coworkers have shown that dynamic propensity does not have a direct relation with several local structural quantities or the potential energy [35, 43]. Rather, spatial distributions of the dynamic propensity turns out to be correlated with the Debye-Waller factor, and agrees with an actual resultant dynamics over a large length scale [35]. Appignanesi and coworkers have shown that the dynamic propensity closely reflects the structural constraints of the system at an initial configuration as long as the timescale is not much larger than the relaxation timescale [38–41]. In this study, we set the time interval t^* to be $1.5\tau_\alpha$ as done in the previous studies [36]. Discussions on the use of different values of the time scale will be made later.

III. MODEL DESCRIPTION AND SIMULATION METHODS

To achieve good statistics necessary for computing the dynamic propensity at low temperatures, it is convenient to introduce a coarse-grained model of an RTIL.

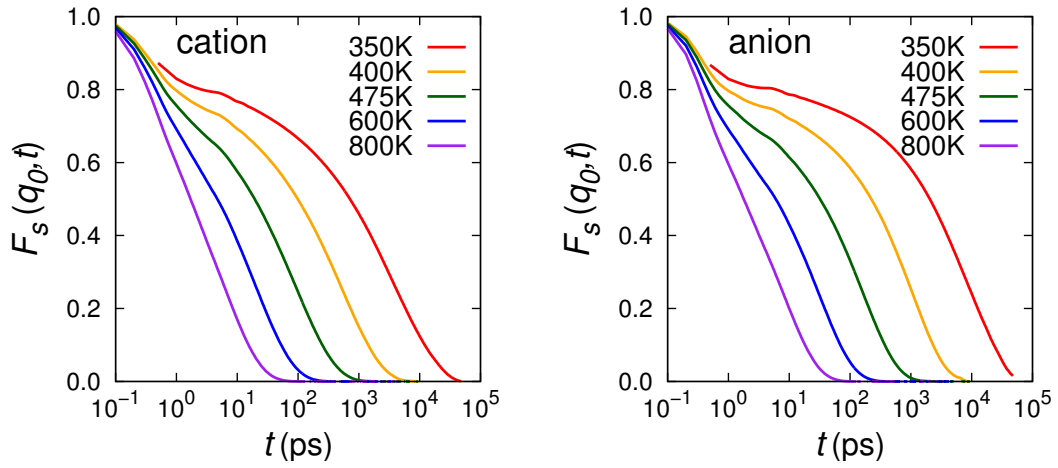

FIG. 1: Self-intermediate scattering fuction $F_s(q_0, t)$ for cations (left) and anions (right) at various temperatures. The wave vector q_0 is given by $1.24\,\text{Å}^{-1}$. τ_α's for the cations and anions are compiled in Table I.

We employ a simple model of the RTIL, 1-ethyl-3-methylimidazolium hexafluorophosphate ($EMI^+PF_6^-$), which has been introduced in previous studies [15]. In this model, the cation, EMI^+, is represented by a rigid molecule consisting of four united atoms, while the anion, PF_6^-, a single united atom. The system consists of 512 pairs of cations and anions confined in a cubic box of length 55.0 Å, where the density is set to be $1.31\,\text{g/cm}^3$. For the Lennard-Jones parameters and partial charges of the united atoms, the reader is referred to Ref. 15.

Molecular dynamics (MD) simulations were conducted in the NVT ensemble through the use of the DL_POLY simulation package. We have used the Nosé-Hoover thermostat and employed the Verlet-leapfrog algorithm with a time step of 2 fs for numerical integrations. Long-range electrostatic interactions were computed with the Ewald summation method.

In preparation for obtaining the dynamic propensity, we produce equilibrium configurations at various temperatures and determine the time interval t^* defined in Eq. 1. Initially, we generate five different equilibrium configurations at $T = 800\,\text{K}$, of which subsequent ones were separated by 2 ns interval, long enough

TABLE I: Structural relaxation time τ_α for the cations(+) and anions(-) at various temperatures T. τ_α and T are in unit of ps and K, respectively.

T	τ_α(+)	τ_α(-)
350	1960	4840
400	262	538
475	48.2	80.8
600	11.1	14.9
800	3.4	3.9

to make them statistically uncorrelated from each other. When equilibrating the system at lower temperatures, an initial configuration is taken as one of the equilibrium configurations at the nearest higher temperature. In this manner, we obtain five equilibrium configurations at each temperature of $T = 600\,\mathrm{K}$, $475\,\mathrm{K}$, $400\,\mathrm{K}$, and $350\,\mathrm{K}$. Then, we perform MD simulations to calculate the self-intermediate scattering function $F_s(q_0, t)$, and obtain the structural relaxation time τ_α for each temperature. Figure 1 shows the intermediate scattering function $F_s(q_0, t)$ averaged over five independent trajectories at different temperatures, where q_0 is set to be $1.24\,\mathrm{\AA}^{-1}$. We set the time interval t^* to be $1.5\tau_\alpha$ as done in the previous studies [36]. τ_α's for the cations and anions at five temperatures are compiled in Table I.

When calculating the dynamic propensity, we produce 200 trajectories at a given configuration with newly assigned momenta, following the MB distribution at each temperature. The dynamic propensity is determined to be the average of squared displacements of each ion during t^*.

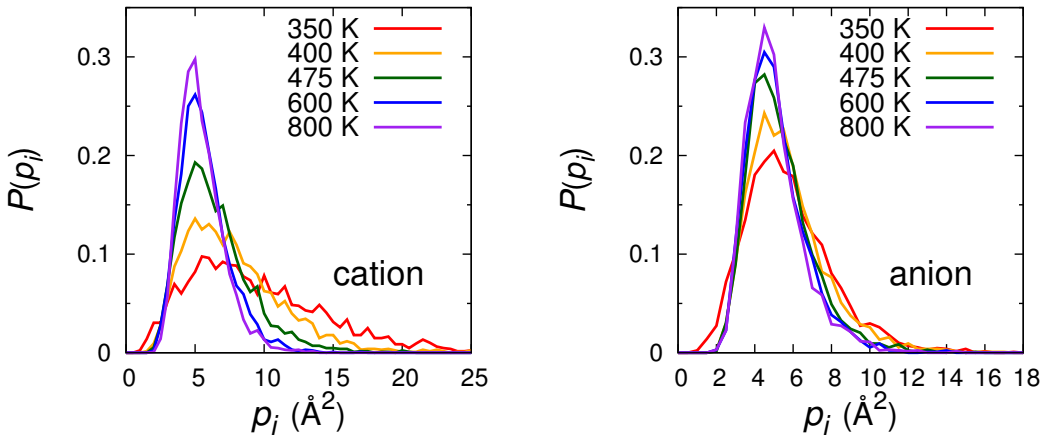

FIG. 2: Distributions of propensity p_i averaged over five configurations for the cations (left) and anions (right) at various temperatures.

IV. RESULTS AND DISCUSSIONS

A. Distributions of dynamic propensity

We have calculated distributions of the dynamic propensity for the cations and anions separately, by taking the averages over the five independent initial configurations. In Fig. 2, the probability distributions $P(p_i)$ of propensities for the cations and anions are presented at five different temperatures. At 800 K, the highest temperature studied, the ions move around relatively freely due to thermal fluctuations. Thus, each ion is in a statistically identical environment during t^*, which results in the Gaussian distribution of $P(p_i)$ according to the central limit theorem. On the other hand, as the temperature is lowered, $P(p_i)$ becomes broad and asymmetric, especially for the case of cations. This suggests that the motions of each ion must have been influenced by different local structures, since the effect of initial momenta in the IC ensemble has already been averaged out. In other words, ions with low propensity are initially in a very restrictive environment, while ions with high propensity are free of such restrictions. This indicates that the distribution of propensity should give information on the development of the

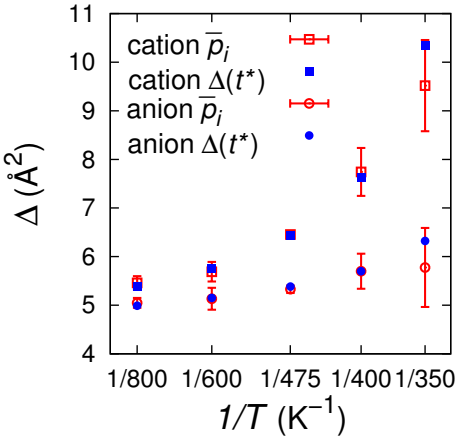

FIG. 3: Mean square displacement $\Delta(t^*)$ and $\overline{p_i}$ for cations and anions at various temperature. Error bars are estimated from the standard deviations of $\overline{p_i}$ for five configurations.

dynamic heterogeneity as the temperature is lowered.

Now we compare the results of the cations and anions. At low temperatures, developments of fat tails in the distribution with decreasing temperature are more prominent in cations than in anions. It implies that environments surrounding the anions are relatively homogeneous than those surrounding the cations. We note that τ_α for the anion is about 2.5 times larger than that of the cation as presented in Sec. III. During the structural relaxation time of the anions, the cations locally arranged around an anion may fully relax, so that the effect of dynamic constraint is averaged out. Moreover, due to the spherical geometry, the anions take part in the local relaxation dynamics less actively than cations. Therefore, dynamics of the cations make more important contributions to the dynamic heterogeneity of our RTIL system.

Sufficiently sampled IC ensemble would reflect the system at equilibrium. If this is the case, $\overline{p_i}$, the averaged propensity over the given ionic species, should be the same as the value of the mean squared displacement (MSD) at time t^*, $\Delta(t^*) \equiv \langle N^{-1} \sum_i |\mathbf{r}_i(t^*) - \mathbf{r}_i(0)|^2 \rangle$. Because the system is in the diffusive regime at

t^*, the mean squared displacement linearly increases with time such that $\Delta(t^*) \approx 6Dt^*$, where D denotes the diffusion coefficient. In the case of normal liquids, the Stokes-Einstein (SE) relation is satisfied and $D\tau_\alpha$ is constant, independent of the temperature. If this is the case, by recalling that $t^* = 1.5\tau_\alpha$ in this work it can be shown that $\overline{p_i} \approx \Delta(t^*) \approx 9D\tau_\alpha$, regardless of the temperature. However, Fig. 3 shows that both $\overline{p_i}$ and $\Delta(t^*)$ increase as the temperature is lowered, and this indicates the violation of the SE relation. It also shows that the dynamics of the cation violates the SE relation more dramatically than that of the anion. This is consistent with the previous observation of the dominant role played by the cations in heterogeneous dynamics.

B. Statistics in the isoconfigurational ensemble

We consider the fluctuations among different trajectories in the IC ensemble. In order to do that, we define σ_i as the standard deviation of squared displacements of i-th ion,

$$\sigma_i = \left[\langle {\Delta r_i}^4 \rangle_{\mathrm{IC}} - \langle {\Delta r_i}^2 \rangle_{\mathrm{IC}}^2\right]^{1/2}. \tag{2}$$

We first focus on the correlation between the propensity and standard deviation. Scatter plots of σ_i and p_i for the cations and anions at 350 K and 800 K are shown in Fig. 4. First of all, we notice that at 350 K, σ_i's show a positive deviation from the result that would be obtained by assuming three-dimensional random walk, $\sigma_i = (2/3)^{1/2} p_i$, represented by a solid line both for cations and anions. At 800 K, however, the data are consistent with the random walk result. These observations suggest that the dynamics of the RTIL at 350 K do not follow simple random walk motions, and instead, there are additional dynamical fluctuations contributing to intermittent, large displacements of ions. At both temperatures,

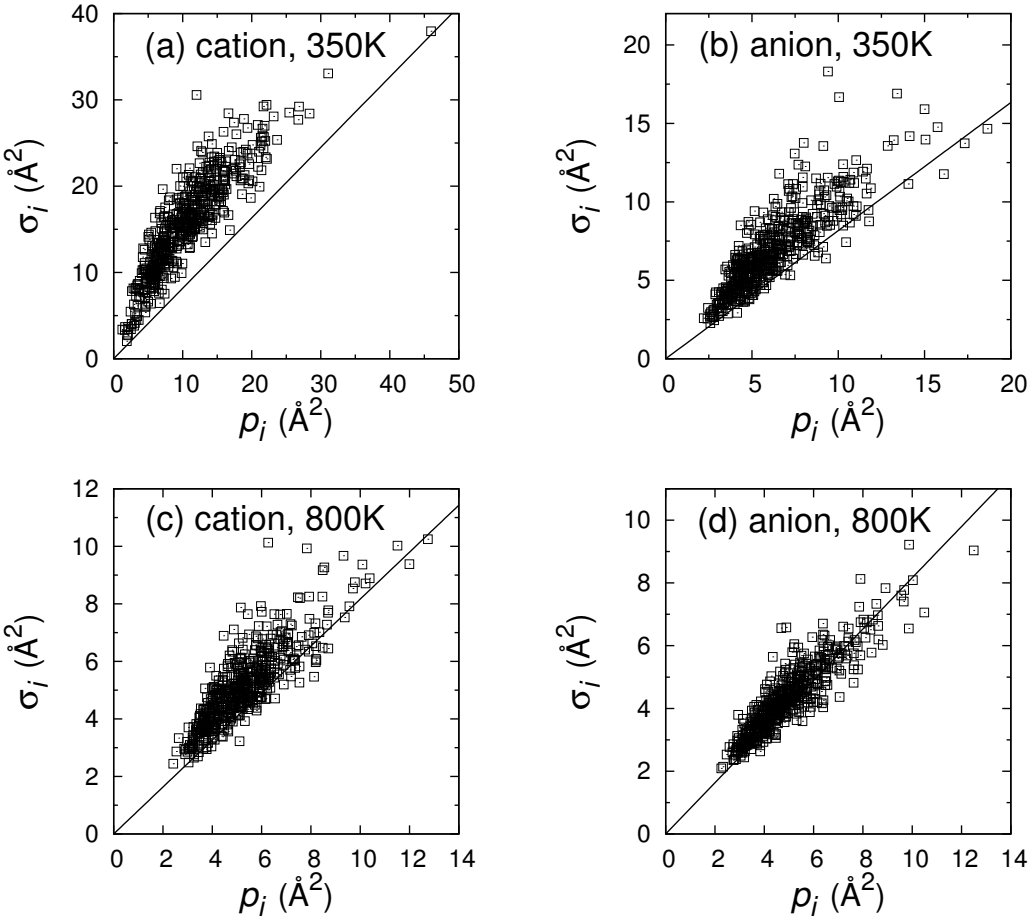

FIG. 4: The correlations between the propensity p_i and the standard deviation of the propensity σ_i for the (a) cations at 350 K, (b) anions at 350 K, (c) cations at 800 K, and (d) anions at 800 K. The solid line indicates the 3D random walk result, $\sigma_i = (2/3)^{1/2} p_i$.

ions (especially cations) with a high propensity generally show large σ_i. This implies that ions with a high propensity does not necessarily mean that they all exhibit large displacements in a given single trajectory.

Based on these observations, it seems important to look at the distributions of the propensity of individual ions, and further to probe possible correlation with other dynamical quantities of ions. Thus, we consider distributions of the displacements of the i-th ion during t^*, denoted by $f_i(\Delta r)$, to further describe the statistics in the IC ensemble. Then, the propensity p_i corresponds to the second moment of $f_i(\Delta r)$. Note that the distribution $f_i(\Delta r)$ is obtained from different

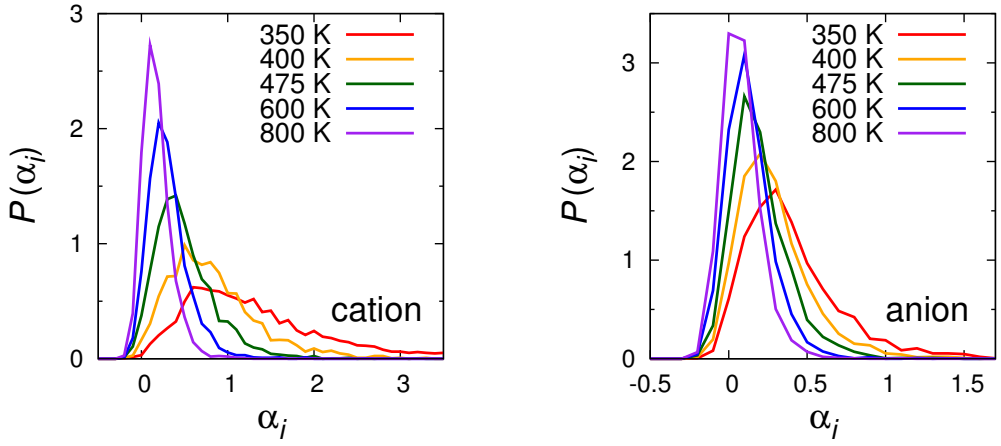

FIG. 5: Distributions of the non-Gaussian parameter α_i averaged over five configurations for cations (left) and anions (right) at various temperatures.

trajectories of the same i-th ion starting from the same initial configuration, and not a quantity averaged over different ions. In order to characterize the distribution $f_i(\Delta r)$, the non-Gaussian parameter α_i is defined to be

$$\alpha_i \equiv \frac{3\langle \Delta r_i^4 \rangle_{\rm IC}}{5\langle \Delta r_i^2 \rangle_{\rm IC}^2} - 1. \tag{3}$$

In Fig. 5, the distributions of α_i for the cations and anions are displayed at five temperatures. At 800 K, the distribution is narrow and its mean value almost vanishes. As the temperature is lowered, the distributions shift to the right with broadening, indicating the increase of non-Gaussianity in the IC ensemble. The deviation of σ_i from the random walk result shown in Fig. 4 is also due to the non-Gaussian character of the IC ensemble at a low temperature.

In the scatter plots of α_i and p_i shown in Fig. 6, the cations with high p_i tend to have rather small values of α_i. On the other hand, for small values of $p_i (\lesssim 10\,\text{Å}^2)$, α_i exhibits a wide variation: α_i is mostly less than 2, but about 14% of the cations exhibit larger values of α_i. This behavior indicates that there is a wide variation in the behavior of individual ion's motions in RTILs. In order to further

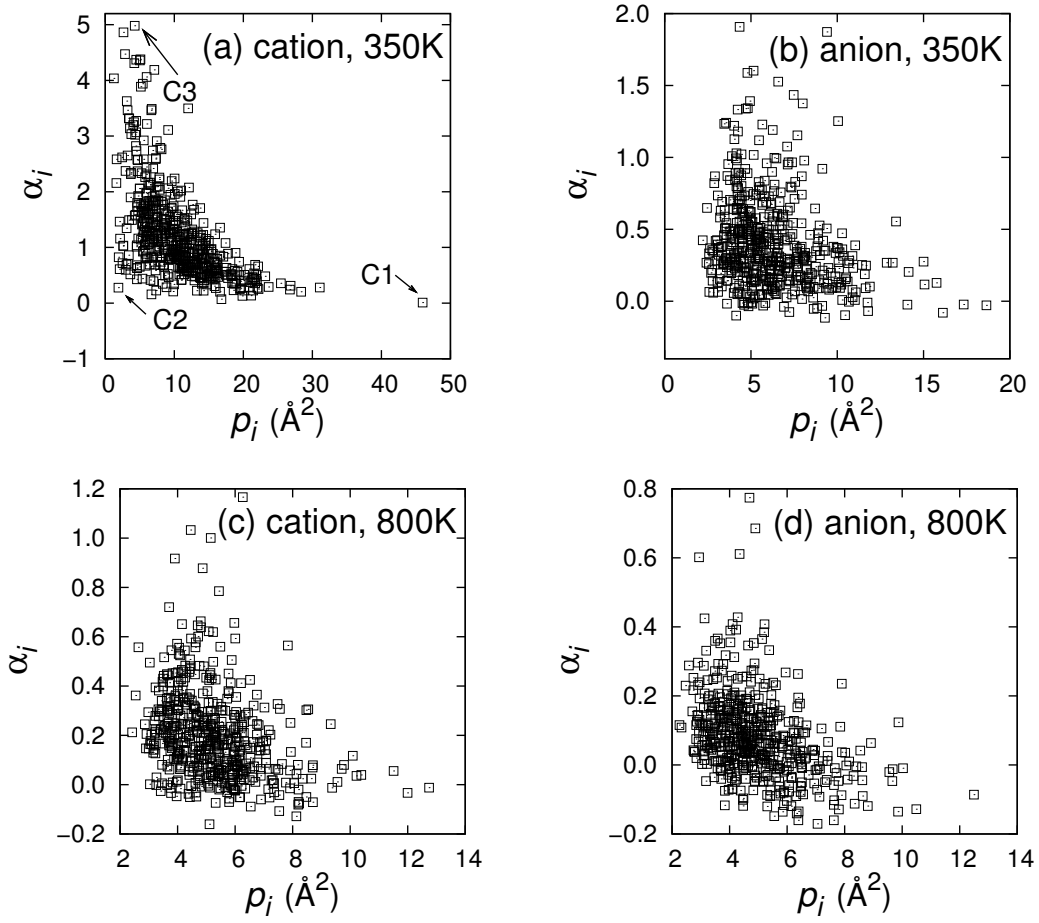

FIG. 6: The correlations between the propensity p_i and the non-Gaussian parameter α_i for the (a) cations at 350 K, (b) anions at 350 K, (c) cations at 800 K, and (d) anions at 800 K.

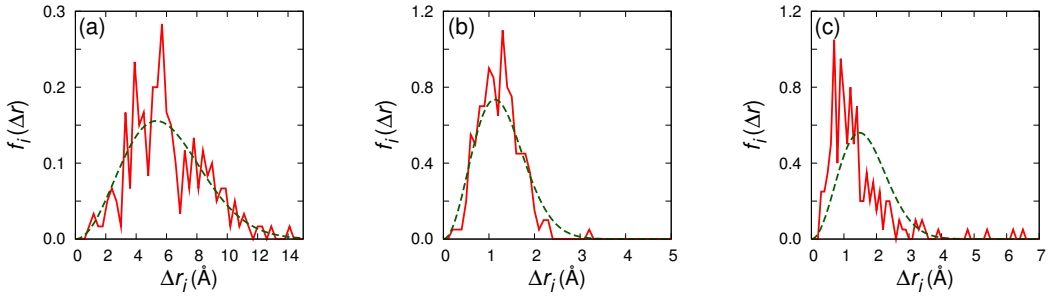

FIG. 7: $f_i(\Delta r)$ in the IC ensemble are shown for three representative cations of (a) C1, (b) C2 , and (c) C3 chosen in Fig. 6 at 350 K. The red (solid) line indicates the original distributions over 200 runs and the green line (dashed) indicates the Gaussian distribution, constructed with the average and standard deviation of the original one.

characterize the statistics of intermittent dynamics of cations, three representative cations marked by C1, C2, and C3 in Fig. 6 are selected. Values of p_i for C1, C2, and C3 are found to be 46.0 Å^2, 1.91 Å^2, and 4.27 Å^2, respectively, and α_i are found to be 0.00873, 0.276, and 4.98. In Fig. 7(a)-(c), $f_i(\Delta r)$ for C1-3 are displayed in the red solid lines. For reference, we show Gaussian distributions, denoted by green dashed lines, which are constructed by using p_i and σ_i, as mean and standard deviation, respectively, for each case. As inferred from the corresponding values of α_i, $f_i(\Delta r)$ for C1 and C2 are almost consistent with $g_i(\Delta r)$, while $f_i(\Delta r)$ for C3 markedly deviates from $g_i(\Delta r)$.

This analysis allows us to infer that different dynamical behaviors would be possible for individual ions. For example, C1 and C2 exhibit Gaussian statistics peaked at high and low propensity value, respectively. This indicates that there are some ions whose dynamics are closely dominated by the initial configuration, mobile for C1 and immobile for C2, up to the time scale of t^*. On the other hand, for the case of C3, the propensity is low but the non-Gaussian parameter is quite large, and the distribution shows clear deviation from the Gaussian. Thus, C3-like cations would have undergone small displacement motions in most of the trajectories, with some exceptions of large displacements in a few trajectories. This is a manifestation of intermittent dynamics arising due to the fluctuation-dominated dynamics of the RTIL [15].

C. Propensity vs. Mobility

In this section, we study how the spatial heterogeneity of dynamic propensity reflects the actual dynamics starting from the same initial configurations. The dynamics of the ions are described by another particle-based quantity, named the mobility in this study. We examine possible correlations and spatial overlaps between the dynamic propensity and mobility obtained from a single run.

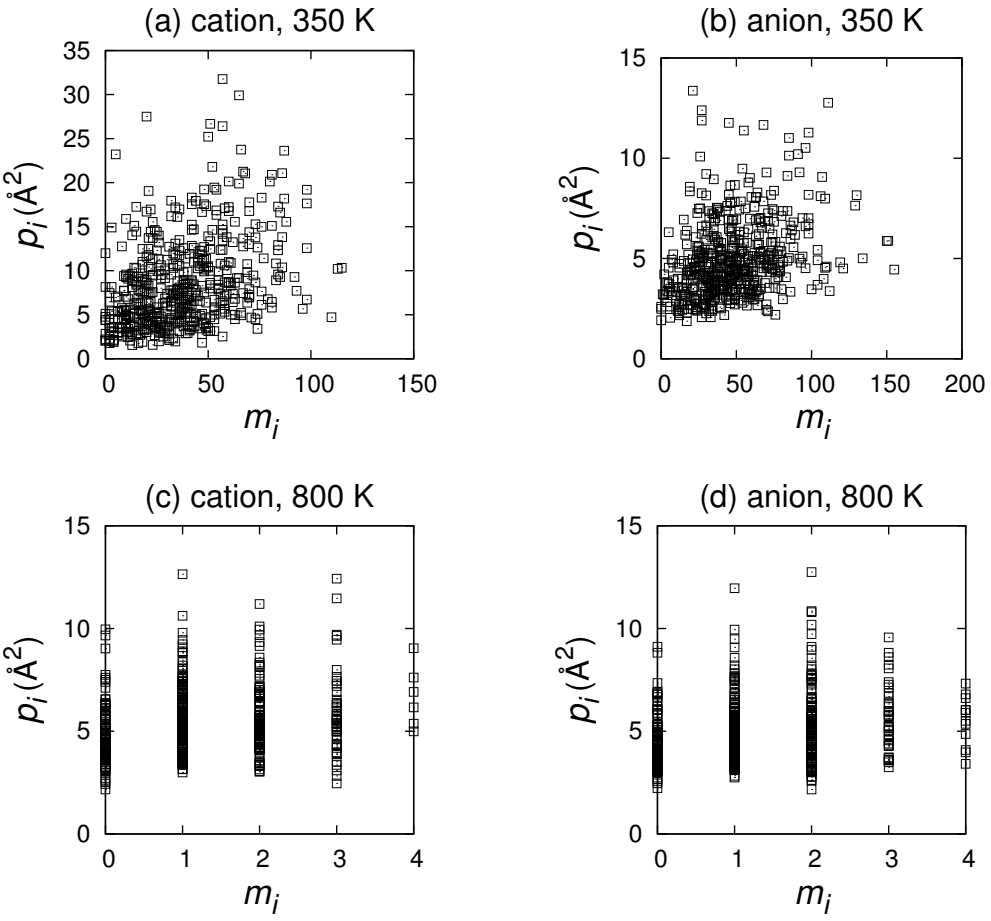

FIG. 8: The correlation plots for the propensity p_i versus the mobility m_i for the (a) cations at 350 K, (b) anions at 350 K, (c) cations at 800 K, and (d) anions at 800 K.

To quantify the motions of each ion in the trajectory, we define the mobility by counting the local excitation events. We regard the displacement of an ion by a distance larger than a threshold distance d as an excitation [15, 29], where d is chosen to be $\sqrt{5}$ Å in this study. To be specific, if the position $\mathbf{r}_i$ for the center of mass of i-th ion follows $|\mathbf{r}_i(t_1) - \mathbf{r}_i(0)| = d$, $|\mathbf{r}_i(t_2) - \mathbf{r}_i(t_1)| = d$, etc., then t_1, $t_2, \cdots$ are identified as the instances of the excitation events. Other choices of d corresponding to the length scale of subdiffusive motion do not change our results in terms of identifying mobile and immobile ions. Effects of the cut off distance d on the average time interval between subsequent excitations were considered in

a previous study [15]. We note that a larger value of d should give more sparse excitations, resulting in the difficulty in the analysis.

The mobility of the i-th ion, denoted by m_i, is defined as the number of excitation events occurred during the time interval t^*. We set t^* to be $1.5\tau_\alpha$, the same as the time interval for calculating the dynamic propensity in the previous section. The heterogeneous dynamics of the RTIL is described by distributions of m_i, which specifies the dynamic state of an ion being mobile or immobile.

In Fig. 8, we present correlation plots of the dynamic propensity p_i and mobility m_i for cations and anions at 350 K and 800 K. Overall, the correlation plot develop a "fan-like" structure. At 350 K, m_i and p_i exhibit weak correlations for cations and anions in Fig. 8(a) and (b), respectively. On the other hand, at 800 K, p_i seems independent of m_i in Fig. 8(c) and (d). Note that at 800 K m_i's are quite small because of short relaxation time.

The correlation between p_i and m_i can be quantified conveniently with the linear correlation coefficient Q, which is defined to be

$$Q \equiv \frac{\overline{\delta p_i \delta m_i}}{\sqrt{\overline{\delta {p_i}^2}}\sqrt{\overline{\delta {m_i}^2}}}, \tag{4}$$

where δp_i and δm_i are $p_i - \overline{p_i}$ and $m_i - \overline{m_i}$, respectively, and overlines denote averaging over the same ionic species. The correlation coefficients Q for cations and anions are found to be 0.43 and 0.35 at 350 K, respectively, while 0.24 and 0.26 at 800 K, which indicates there is rather a weak correlation between the propensity and mobility overall. This tells that dynamic propensity itself is not predictive of the mobility of individual ions.

Although there is an overall, weak correlation between the propensity and mobility, once we focus on the low mobility-low propensity region, rather a strong correlation between the two is observed. To be specific, when the propensity is

below 5 Å^2, we see few data corresponding to the mobility over 60 in Fig. 8(a). Low propensities reflect structural constraints imposed on the initial configuration, resulting immobile region in the subsequent dynamics. On the other hand, ions of higher propensities cover a wide range of mobility. This is consistent with with the results of Sec. IV B, that is, the standard deviation of the displacement for an ion calculated in the IC ensemble increases with p_i, and a high p_i for an ion provides little information about the motions of the ion in a single run.

In fact, connections between high propensity and mobility regions have been developed previously in the case of atomic liquid systems [38–41]. In atomic liquid systems, it has been shown that glassy systems relax through sequences of intermittent, large scale excitation events, and when these happen, patterns of the dynamic propensity lose their correlations. Physically, this would correspond to transitions between different metabasins of liquid configurations. When this event happens, new patterns of dynamic propensity develops, utilizing more mobile regions for the next relaxation events. While there is a whole distribution of timescales, it is known that the typical timescales of such events are on the order of the metabasin lifetime, shorter than the structural relaxation time.

Thus, one can imagine the following scenario. In the heterogeneous dynamics of the RTIL, the system loses the pattern of initial constraints with widely distributed time scales. In the region where the initial constraints decorrelates fast, the actual dynamics becomes rather independent of the initial structure, while in the region where they decorrelate slowly, the correlation between the mobility and propensity is preserved. Note that this decorrelation pattern would depend upon the time scale used, which is chosen as $t^* = 1.5\tau_\alpha$ in this study. Thus, it seems plausible to correlate different types of dynamical behaviors of cations, classified as C1–C3 in Sec. IV B to different cases of decorrelation patterns of dynamic propensities, which is certainly subject to more thorough investigation.

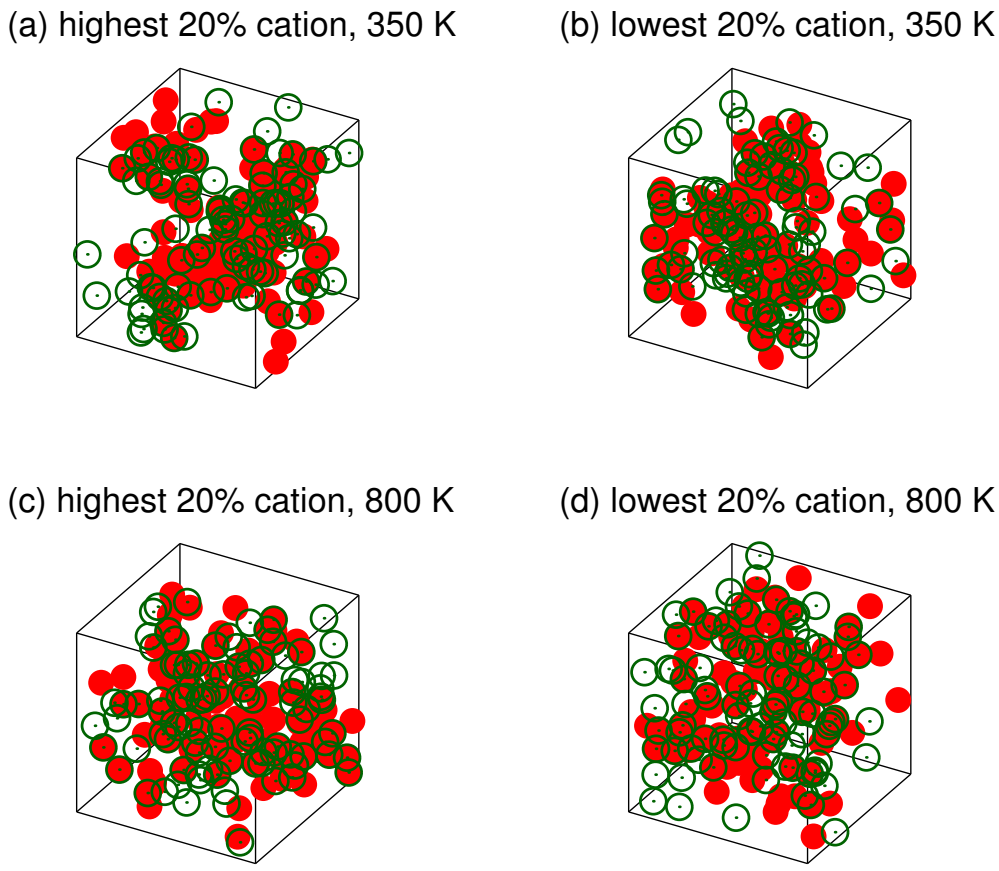

FIG. 9: Spatial overlap between propensity (filled red circles) and mobility (empty green circles) for the cases of (a) highest 20 % cations at 350 K, (b) lowest 20% cations at 350 K (c) highest 20 % cations at 800 K, (d) lowest 20 % cations at 800 K

Although one needs to check if the above scenario really applies to more complex liquid systems such as RTILs studied in this work, our results seem to be consistent with this picture, and it could possibly be the reason why we find rather weak correlation between the propensity and mobility when they are calculated at the time scale $t^* = 1.5\tau_\alpha$. Certainly it would be interesting to see how the correlation between the two quantities vary when the timescale becomes shorter.

Though we have not observed distinct correlations between p_i and m_i of all ions, we expect that they may develop spatial correlations in their distribution patterns. We thus present overlap of spatial distributions of ions with higher (or lower) p_i

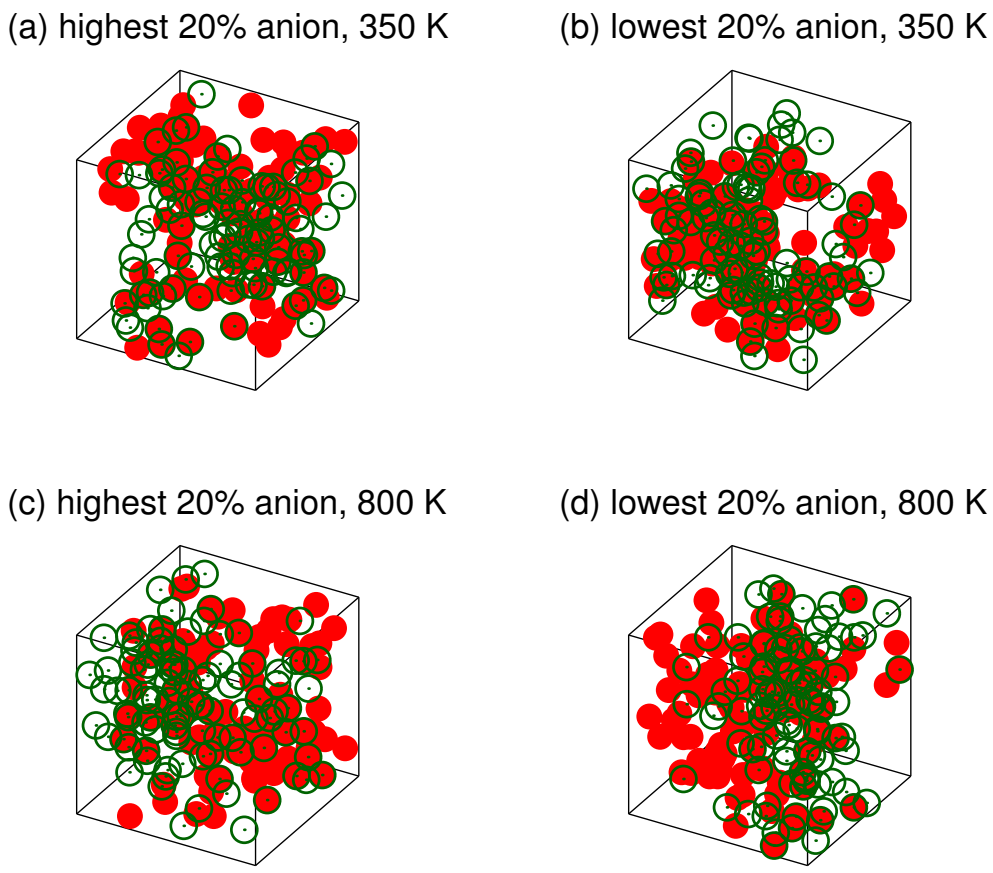

FIG. 10: Spatial overlap between propensity (filled red circles) and mobility (empty green circles) for the cases of (a) highest 20 % anions at 350 K, (b) lowest 20 % anions at 350 K, (c) highest 20 % anions at 800 K, and (d) lowest 20 % anions at 800 K.

together with those with higher (or smaller) m_i for an initial configuration at 350 K and 800 K, both for cations in Fig. 9 and for anions in Fig. 10, respectively. In these figures, filled red circles represent ions with highest (or lowest) 20% of propensities, while empty green circles represent those with highest (or lowest) 20% of mobilities, respectively. The radii of all particles are set to be same. It is clear that at 350 K ions with high propensities are distributed forming clusters. Moreover, ions with high mobility indeed show strong correlation with those with high propensity. This is not the case at a higher temperature of 800 K.

V. CONCLUSIONS

We investigated the dynamic propensity in a model RTIL system via molecular dynamics simulations in this work. It turns out that our RTIL model system also exhibits heterogeneous distributions of the dynamic propensity at room temperatures. We find that as the temperature is lowered, the dynamic propensity develops broad distributions, which indicates the significance of dynamic heterogeneity in the relaxation dynamics of the system. We also find that cations play more dominant roles in the development of the dynamic heterogeneity than anions.

We tried to address an important issue on the dynamic propensity: how it reflects heterogeneous dynamics in RTILs. By observing the statistical quantities in the isoconfigurational ensemble, we observed that the dynamic propensity do not show strong correlation with the mobility at the timescale used in this work. This finding is certainly consistent with previous results obtained in the atomic liquid systems [38–41]. It would be an important and intriguing issue to probe how the correlation between the two quantities vary as the timescale changes.

While we do not find the strong correlation between the propensity and the mobility based on individual ions, spatial patterns of the high (or low) propensity ions seem to be correlated with those of mobile (or immobile) regions, respectively. Although more detailed analysis of spatial patterns of mobility/propensity distributions may be necessary, our observation implies that any structural aspects relevant to spatial heterogeneity of the dynamics should involve length scales larger than inter-ion distances, which is in agreement with a previous study [37]. Along this line, we will perform further studies regarding the length scale of the heterogeneity and the possibility of the long-ranged structural properties.

Acknowledgement

This work was supported by the National Research Foundation of Korea(NRF) grants funded by the Korea government (Nos. 2007-0056095 and 2012-R1A1A2042062).

[1] J. D. Holbrey and K. R. Seddon, *Clean Products Processes*, 1999, **1**, 223.

[2] P. Wasserscheid and W. Keim, *Angew. Chem. Int. Ed.*, 2000, **39**, 3772.

[3] H. Weingärtner, *Angew. Chem. Int. Ed.*, 2008, **47**, 654.

[4] A. Noda, A. B. Kubo, S. Mitsushima, K. Hayamizu and M. Watanabe, *J. Phys. Chem. B*, 2003, **107**, 4024.

[5] P. Wang, S. M. Zakeeruddin, J.-E. Moser and M. Grätzel, *J. Phys. Chem. B*, 2003, **107**, 13280.

[6] T. Tsuda and C. L. Hussey, *Interface*, 2007, **16**, 42.

[7] J. Wang, Y. Tian, Y. Zhao and K. Zhuo, *Green Chemistry*, 2003, **5**, 618.

[8] N. Ito and R. Richert, *J. Phys. Chem. B*, 2007, **111**, 5016.

[9] (*a*) Y. Shim, J. Duan, M. Y. Choi and H. J. Kim, *J. Chem. Phys.*, 2003, **119**, 6411; (*b*) Y. Shim, M. Y. Choi and H. J. Kim, *J. Chem. Phys.*, 2005, **122**, 044510; (*c*) Y. Shim, M. Y. Choi and H. J. Kim, *J. Chem. Phys.*, 2005, **122**, 044511.

[10] Y. Shim, D. Jeong, M. Y. Choi and H. J. Kim, *J. Chem. Phys.*, 2006, **125**, 061102.

[11] Y. Shim, D. Jeong, S. Manjari, M. Y. Choi and H. J. Kim, *Acc. Chem. Res.*, 2007, **40**, 1130.

[12] Y. Shim and H. J. Kim, *J. Phys. Chem. B*, 2010, **114**, 10160.

[13] D. Jeong, Y. Shim, M. Y. Choi and H. J. Kim, *J. Phys. Chem. B*, 2007, **111**, 4920.

[14] D. Jeong, Y. Jung, M. Y. Choi and H. J. Kim, *J. Chem. Phys.*, 2008, **128**, 174504.

[15] D. Jeong, M. Y. Choi, H. J. Kim and Y. Jung, *Phys. Chem. Chem. Phys.*, 2010,

12, 2001.

[16] (*a*) C. J. Margulis, *Mol. Phys.*, 2004, **102**, 829; (*b*) Z. Hu and C. J. Margulis, *Proc. Natl. Acad. Sci. U.S.A.*, 2006, **103**, 831; (*c*) Z. Hu and C. J. Margulis, *J. Phys. Chem. B*, 2006, **110**, 11025.

[17] B. L. Bhargava and S. Balasubramanian, *J. Chem. Phys.*, 2005, **123**, 144505.

[18] (*a*) M. N. Kobrak and Z. Znamenskiy, *Chem. Phys. Lett.*, 2004, **395**, 127; (*b*) M. N. Kobrak, *J. Chem. Phys.*, 2006, **125**, 064502; (*c*) M. N. Kobrak, *J. Chem. Phys.*, 2007, **127**, 184507.

[19] (*a*) R. Karmakar and A. Samanta, *J. Phys. Chem. A*, 2002, **106**, 4447; (*b*) R. Karmakar and A. Samanta, *J. Phys. Chem. A*, 2002, **106**, 6670; (*c*) R. Karmakar and A. Samanta, *J. Phys. Chem. A*, 2003, **107**, 7340; (*d*) A. Samanta, *J. Phys. Chem. B*, 2006, **110**, 13704; (*e*) A. Samanta, *J. Phys. Chem. Lett.*, 2010, **1**, 1557; (*f*) D. C. Khara and A. Samanta, *indian. J. Chem.*, 2010, **714**, 49A.

[20] (*a*) N. Ito, S. Arzhantsev and M. Maroncelli, *Chem. Phys. Lett.*, 2004, **396**, 83; (*b*) M. Maroncelli, X.-X. Zhang, M. Liang, D. Roy and N. P. Ernsting, *Faraday Discuss. Chem. Soc.*, 2012, **154**, 409; (*c*) D. Roy and M. Maroncelli, *J. Phys. Chem. B*, 2012, **116**, 5951; (*d*) X.-X. Zhang, M. Liang, N. P. Ernsting and M. Maroncelli, *J. Phys. Chem. B*, 2013, **117**, 4291; (*e*) X.-X. Zhang, M. Liang, N. P. Ernsting and M. Maroncelli, *J. Phys. Chem. Lett.*, 2013, **4**, 1205.

[21] (*a*) J. F. Wishart and E. W. Castner, *J. Phys. Chem. B*, 2007, **111**, 4639; (*b*) J. F. Wishart and E. W. Castner, *J. Phys. Chem. B*, 2007, **111**, 4963.

[22] B. Lang, G. Angulo and E. Vauthey, *J. Phys. Chem. A*, 2006, **110**, 7028.

[23] H. Cang, J. Li and M. D. Fayer, *J. Chem. Phys.*, 2003, **119**, 13017.

[24] Y. Jung, J. P. Garrahan and D. Chandler, *Phys. Rev. E*, 2004, **69**, 061205.

[25] Y. Jung, J. P. Garrahan and D. Chandler, *J. Chem. Phys.*, 2005, **123**, 084509.

[26] G. Tarjus and D. Kivelson, *J. Chem. Phys.*, 1995, **103**, 3071.

[27] M. G. Mazza, N. Giovambattista, H. E. Stanley and F. W. Starr, *Phys. Rev. E*, 2007, **76**, 031203.

[28] P. Chaudhuri, L. Berthier and W. Kob, *Phys. Rev. Lett.*, 2007, **99**, 060604.

[29] L. O. Hedges, L. Maibaum, D. Chandler and J. P. Garrahan, *J. Chem. Phys.*, 2007, **127**, 211101.

[30] S. Léonard and L. Berthier, *J. Phys.:Condens. Matter*, 2005, **17**, S3571.

[31] J. P. Garrahan and D. Chandler, *Phys. Rev. Lett.*, 2002, **89**, 035704.

[32] M. Merolle, J. P. Garrahan and D. Chandler, *Proc. Natl. Acad. Sci. USA*, 2005, **102**, 10837.

[33] A. Widmer-Cooper, H. Perry, P. Harrowell and D. R. Reichman, *Nature Physics*, 2008, **4**, 711.

[34] A. Widmer-Cooper, P. Harrowell and H. Fynewever, *Phys. Rev. Lett.*, 2004, **93**, 135701.

[35] A. Widmer-Cooper and P. Harrowell, *Phys. Rev. Lett.*, 2006, **96**, 185701.

[36] A. Widmer-Cooper and P. Harrowell, *J. Chem. Phys.*, 2007, **126**, 154503.

[37] L. Berthier and R. L. Jack, *Phys. Rev. E*, 2007, **76**, 041509.

[38] J. A. Rodriguez Fris, L. M. Alarcón, and G. A. Appignanesi, *Phys. Rev. E*, 2007, **76**, 011502.

[39] J. A. Rodrigues Fris, L. M. Alarcón and G. A. Appignanesi, *J. Chem. Phys.*, 2009, **130**, 024108.

[40] M. A. Frechero, L. M. Alarcón, E. P. Schulz and G. A. Appignanesi, *Phys. Rev. E*, 2007, **75**, 011502.

[41] J. A. Rodriguez Fris, G. A. Appignanesi and E. R. Weeks, *Phys. Rev. Lett*, 2011, **107**, 065704.

[42] L. O. Hedges and J. P. Garrahan, *J. Phys.:Condens. Matter*, 2007, **19**, 205124.

[43] A. Widmer-Cooper and P. Harrowell, *J. Phys.:Condens. Matter*, 2005, **17**, S4025.

Table of Contents

Dynamic propensity of an RTIL system exhibits broad and asymmetric distributions, and spatial patterns of the dynamic propensity and mobility distribution are shown.